FULL PAPER

Anode-Free Rechargeable Lithium Metal Batteries

Jiangfeng Qian, Brian D. Adams, Jianming Zheng, Wu Xu, Wesley A. Henderson, Jun Wang, Mark E. Bowden, Suochang Xu, Jianzhi Hu, and Ji-Guang Zhang*

Anode-free rechargeable lithium (Li) batteries (AFLBs) are phenomenal energy storage systems due to their significantly increased energy density and reduced cost relative to Li-ion batteries, as well as ease of assembly because of the absence of an active (reactive) anode material. However, significant challenges, including Li dendrite growth and low cycling Coulombic efficiency (CE), have prevented their practical implementation. Here, an anode-free rechargeable lithium battery based on a Cu||LiFePO$_4$ cell structure with an extremely high CE (>99.8%) is reported for the first time. This results from the utilization of both an exceptionally stable electrolyte and optimized charge/discharge protocols, which minimize the corrosion of the in situly formed Li metal anode.

1. Introduction

Batteries with high energy density, long cycle life, and low cost are key enablers for consumer electronics, electric vehicles (EVs), and smart grid energy storage.[1–4] To date, lithium (Li)-ion batteries have been one of the most widely used energy storage systems. A commercial Li-ion battery consists of multiple cell stacks—each composed of an anode current collector/anode/separator/cathode/cathode current collector—soaked with a liquid electrolyte (typically 1 M LiPF$_6$ in carbonate solvent mixtures). Common configurations for Li-ion batteries used in commercial electronics include: Cu/graphite/separator/LiCoO$_2$/Al and Cu/graphite/separator/LiFePO$_4$/Al.[5,6] For such

batteries, during the charge process, the Li$^+$ ions extracted from the cathode materials diffuse through the electrolyte-soaked separator, and then intercalate into the anode material (i.e., graphite). The process is reversed during the discharge process. In these batteries, the usable energy is determined by the identity and amount of active materials present, but the total weight and to a large extent cost are determined by all of the materials, with sizeable contributions from the inactive components such as the separator, current collectors, and packaging materials.

Ideally, if the Li$^+$ ions extracted from a cathode can be reversibly plated onto and stripped from a Cu current collector (as Li metal), then it is possible to assemble a rechargeable Li battery with a Cu/separator/cathode/Al configuration. When initially assembled, this battery contains no active anode material and thus can be referred to as an "anode-free rechargeable lithium metal battery (AFLB)." A schematic illustration of an AFLB is shown in **Figure 1**b, where a state-of-the-art Li-ion battery (Figure 1a) is shown for reference. In the anode-free configuration, all of the active Li$^+$ ions are initially stored in the cathode (Figure 1a) endowing this design with several key advantages. Notably, the absence of an Li$^+$ host anode material reduces the cell weight and space required for the graphite. In a typical Li-ion battery (Figure 1a), the cathode thickness is comparable to that of the graphite anode. The energy density of the AFLB will therefore be significantly larger than that for conventional Li-ion batteries, even when the increased thickness due to Li plating when the battery is charged is considered,[7] since the theoretical capacity of Li (3820 mAh cm^{-2}) is more than ten times that of graphite (372 mAh cm^{-2}) resulting in a potential increase in the energy density (Wh L^{-1}) of AFLBs by more than ≈50% relative to conventional Li-ion batteries. In addition, the energy and cost associated with anode production (including electrode slurry preparation, slurry coating, and drying) are saved. Finally, the anode-free design operates as an Li metal battery after the initial charge process, thus providing a higher (≈0.1 V) operating voltage and thus higher energy density (the product of the active material capacity and cell voltage) than for conventional Li-ion batteries.

During the initial charge process of an AFLB, Li$^+$ ions are extracted from the cathode and transported toward the anode current collector where they are electroplated as metallic Li. During the subsequent discharge process, Li will be stripped from the anode and intercalated back into the cathode.[8–10] Traditionally, this optimal battery configuration (no excess Li in the cell) was considered to be unworkable. In addition to the concern of dendritic Li growth, resulting in dendrite penetration

Dr. J. Qian, Dr. B. D. Adams, Dr. W. Xu,
Dr. J. Hu, Dr. J.-G. Zhang
The Joint Center for Energy Storage Research (JCESR)
Pacific Northwest National Laboratory
Richland, WA 99354, USA
E-mail: jiguang.zhang@pnnl.gov
Dr. J. Qian, Dr. B. D. Adams, Dr. J. Zheng,
Dr. W. Xu, Dr. W. A. Henderson, Dr. J.-G. Zhang
Energy and Environment Directorate
Pacific Northwest National Laboratory
Richland, WA 99354, USA
Dr. J. Wang
A123 Systems Research and Development
Waltham, MA 02451, USA
Dr. M. E. Bowden
Environmental and Molecular Sciences Laboratory
Pacific Northwest National Laboratory
Richland, WA 99354, USA
Dr. S. Xu, Dr. J. Hu
Earth and Biological Science Directorate
Pacific Northwest National Laboratory
Richland, WA 99354, USA

www.MaterialsViews.com

ADVANCED
FUNCTIONAL
MATERIALS
www.afm-journal.de

FULL PAPER
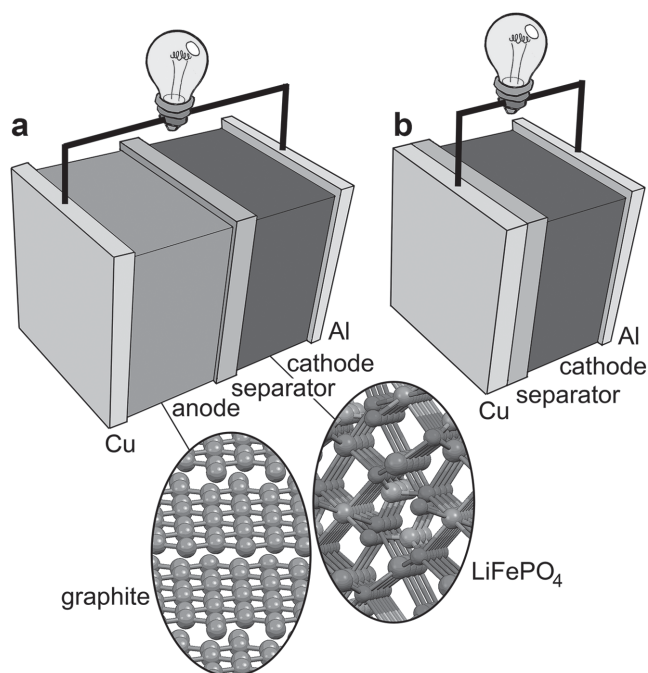
Figure 1. Schematic illustrations of battery configurations. a) State-of-the-art Li-ion battery, i.e., Cu|C$_6$||LiFePO$_4$|Al. b) Anode-free battery, i.e., Cu||LiFePO$_4$|Al.

through the separator and shorting of the cell,[4,11,12] the direct use of Li metal is highly problematic due to its high reactivity and thus typically very low plating/stripping efficiency—usually less than 80% in most non-aqueous electrolytes. As a consequence, the in situ plated Li supplied by the cathode will be completely consumed within a few cycles. In this regard, the key to realizing the anode-free concept is the development of a functional electrolyte in which the Li plating/stripping process is dendrite-free and has a high Coulombic efficiency (CE), thereby effecting an exceptional cycling stability. **Table 1** shows the projected cycle life of a battery as a function of Li cycling CE. Here we assume that the cathode of the battery has no degradation and that battery failure occurs if the battery capacity drops below 80% of the original value. For a CE of 99%, the battery has a lifetime of only 22 cycles. For a rechargeable battery to withstand extensive cycling (e.g., >100 cycles), a CE of at least 99.8% is required. Further increases in the CE produce a dramatic boost in the battery's life.

Table 1. Cycle life dependence on CE (to retain 80% of the battery capacity).

CE [%]	Cycles to maintain a capacity > 80% of initial value
99	22
99.1	25
99.7	74
99.8	112
99.9	223
99.99	2231

The use of solid-state electrolytes such as LiPON has been regarded as a promising solution for anode-free batteries, owing to their compatibility with Li.[13–16] However, the intrinsically low conductivity of LiPON and its high cost have limited its application in batteries to those with thin film electrodes with an areal capacity of ≈100 µAh cm^{-2},[14,15,17] suitable principally for microelectronic devices.[13] A liquid organic solvent-based electrolyte with high conductivity and wettability must instead be used for thick electrodes in Li metal cells. But, the traditional carbonate-based electrolyte systems have poor compatibility with Li metal, i.e., inducing Li dendrite growth and a low cycling CE, and are therefore unsuitable for an anode-free cell design.[3,4,18] For example, when a Copper/LiNi$_{1/3}$Mn$_{1/3}$Co$_{1/3}$O$_2$ (NMC) cell was cycled in an electrolyte consists of 1.2 M LiPF$_6$ in ethylene carbonate (EC):ethyl methyl carbonate (EMC) (30:70 wt%), the first cycle loss is as high as 77%. Therefore, this electrolyte is not suitable to be used in an anode-free rechargeable Li battery.[18]

Our previous work, however, demonstrated that highly concentrated electrolytes composed of ether solvents and the lithium bis(fluorosulfonyl)imide (LiFSI) salt enable high rate cycling of an Li metal anode with a high CE (up to 99.1%) without dendrite growth.[19] This was ascribed to the lower amount of solvent present (relative to dilute electrolytes), the absence of uncoordinated solvent, the high anion content, and the improved availability of Li$^+$ ions in the electrolyte. Here we report an anode-free cell design (Cu||LiFePO$_4$) using this highly concentrated electrolyte composed of 1,2-dimethoxyethane (DME) solvent and a high concentration of the LiFSI salt. Importantly, we demonstrate that, in addition to the electrolyte's favorable characteristics, the cycling protocol of the batteries is also a critical factor for enhancing the long-term cycling stability of AFLBs. These cells, when cycled with an optimized charge/discharge protocol, deliver high initial discharge capacities and an average CE of greater than 99.8% during cycling, i.e., the best performance ever reported for anode-free cells with a liquid electrolyte.

2. Results and Discussion

2.1. Electrochemical Properties

As a proof-of-concept, Cu||LiFePO$_4$ coin-type cells were assembled with a Cu anode current collector and an LiFePO$_4$ electrode with a nominal areal capacity of 1.6 mAh cm^{-2} used as the cathode. Two different electrolytes—a conventional carbonate-based electrolyte (1 M LiPF$_6$-EC/DMC (1/2 v/v)) and the highly concentrated ether-based electrolyte (4 M LiFSI-DME)—were used to evaluate the cell performance. For both electrolytes, the Cu||LiFePO$_4$ cells had an initial charge (Li plating on Cu) capacity of ≈1.71 mAh cm^{-2} (**Figure 2**a), corresponding to a specific capacity of 148 mAh g^{-1} (the theoretical capacity of a LiFePO$_4$ cathode is 170 mAh g^{-1}). This indicates that the extent of the Li$^+$ ion extraction from the LiFePO$_4$ cathode (converting its composition to Li$_{1-x}$FePO$_4$) during the initial charge process was equivalent regardless of the electrolyte composition. However, for the cell with the carbonate-based electrolyte, the subsequent discharge process only recovered ≈25% of the
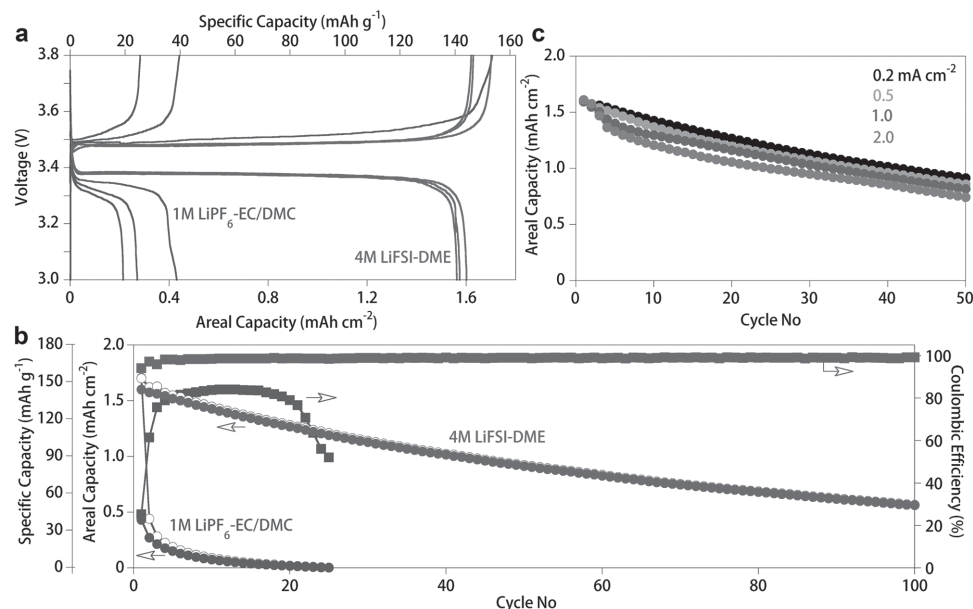
Figure 2. Electrochemical performance of anode-free Cu‖LiFePO$_4$ cells with either 1 M LiPF$_6$-EC/DMC or 4 M LiFSI-DME. a) Charge/discharge voltage profiles for the first three cycles with the two electrolytes. b) Capacity retention and CE of the cells with the two electrolytes as a function of cycle number when charged/discharged at 0.2 mA cm^{-2} (open symbols: charge capacity, filled symbols: discharge capacity). c) Capacity retention of the cells with 4 M LiFSI-DME charged/discharged at different current densities.

total plated Li (re-intercalated into the Li$_{1-x}$FePO$_4$ cathode). The poor reversibility of Li in the carbonate electrolyte is in agreement with recent work reported by Woo et al.,[18] where a Cu‖LiNi$_{1/3}$Mn$_{1/3}$Co$_{1/3}$O$_2$ cell only recovered 23% of the plated Li back into the Li$_{1-x}$Ni$_{1/3}$Mn$_{1/3}$Co$_{1/3}$O$_2$ cathode when using a 1.2 M LiPF$_6$-EC/EMC (3/7 w/w) electrolyte. This tremendous capacity loss is attributed to both the degradation of the active Li material and the resultant formation of a high impedance interphasial layer on the Li metal surface when the plated Li extensively reacts with the carbonate solvents and LiPF$_6$ salt.[18,20] For Li plating in carbonate electrolytes, the plated Li typically grows into dendritic or mossy structures, with a large surface-to-volume ratio.[11] During the stripping process, the Li metal encased within a solid electrolyte interphase (SEI) layer becoming electrically isolated and thus electrochemically inactive, i.e., "dead Li," which is inaccessible for the subsequent plating/stripping processes.[21] This leads to the quick escalation of the cell impedance (**Figure 3**) due to the mossy/dead Li buildup and total failure of the cell occurs after only limited cycling (Figure 2b).

In contrast, the Cu‖LiFePO$_4$ cell with the highly concentrated ether-based electrolyte (4 M LiFSI-DME) had initial charge/discharge capacities of 148/143 mAh g^{-1}, thus providing a high initial CE of 96.6%. This highly reversible capacity remains stable without significant capacity degradation during the first three cycles (Figure 2a), suggesting that the active Li is not consumed during the Li plating/stripping processes. The superior stability of Li in the anode-free cell using the 4 M LiFSI-DME electrolyte is further evidenced by the significantly enhanced capacity retention and higher CE during long-term cycling (Figure 2b). Moreover, a very limited cell impedance increase occurs during the cycling of this cell (Figure 3). Notably, the anode-free cell with the 4 M LiFSI-DME electrolyte retains a

capacity of 85 mAh g^{-1} after 50 cycles (≈60% capacity retention with an average CE > 99%). Even more remarkably, the charge/discharge performance at different current densities demonstrates that the anode-free Cu‖LiFePO$_4$ cell with the 4 M LiFSI-DME electrolyte can be discharged at a rate of 2.0 mA cm^{-2} with near 100% capacity retention, indicating that a very high rate capability is achievable when using the highly concentrated electrolyte. An increase in the charge/discharge current densities, however, results in a slight decrease in the long-term cycling stability of the anode-free cell (Figure 2c), likely due to the slightly lower cycling CE at increased current density.[22]

In addition to the electrolyte formulation, this makes clear that the cycling protocol utilized also plays an important role in the CE of Li cycling. Using an optimized cycling protocol, the cycling CE and capacity retention of the anode-free cells can be further improved. As previously reported for
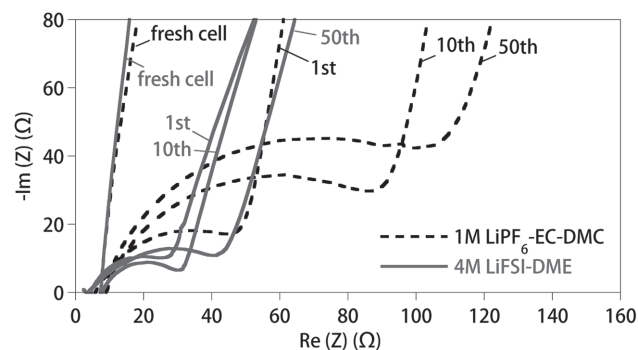
Figure 3. Nyquist plot of anode-free Cu‖LiFePO$_4$ cells with either 1 M LiPF$_6$-EC/DMC (dashed line) or 4 M LiFSI-DME (solid line) after different cycles when charged/discharged at 0.2 mA cm^{-2}. All data were collected at discharged state of the cells.

Materials Views
www.MaterialsViews.com

ADVANCED
FUNCTIONAL
MATERIALS
www.afm-journal.de

FULL PAPER

Li||LiNi$_{1/3}$Mn$_{1/3}$Co$_{1/3}$O$_2$ (NMC) cells,[22] by charging the cells (Li plating) slowly and discharging (Li stripping) at a higher rate, the cycle life is improved relative to cells cycled using other conditions such as charging *and* discharging at the same low rate. However, the CE of the Li||LiNi$_{1/3}$Mn$_{1/3}$Co$_{1/3}$O$_2$ cells with 1 M LiPF$_6$-EC/DMC (1/2 v/v) is low (≈80%), thus requiring the use of a large amount of excessive Li metal anode. We report, however, that the combination of the high concentration electrolyte (4 M LiFSI-DME) and an appropriate cycling protocol enables an extremely high CE for Li cycling, as shown below.

The improvement in the Li plating/stripping CE using this variable-rate cycling protocol is displayed in **Figure 4**b. When Li is plated onto and stripped from a Cu substrate at a low current density of 0.2 mA cm^{-2}, the average CE between cycles 10 and 50 is 98.6%. If the Li plating/stripping is instead performed at a higher current density of 2.0 mA cm^{-2}, the average CE between cycles 10 and 50 is decreased to a 97.7% CE. But,

when a variable low rate charge/high rate discharge protocol is instead used (charge or Li plating: 0.2 mA cm^{-2}; discharge or Li stripping: 2.0 mA cm^{-2}), the average CE between cycles 10 and 50 reaches a very high value of 99.6%.

We also found that, in addition to the cycling current rate protocol, the cycling capacity also plays an important role in stabilizing the SEI. In Figure 4b, the Cu||Li cells were charged to a capacity of 0.5 mAh cm^{-2} (Li plating), whereas the Li||LiFePO$_4$ and Cu||LiFePO$_4$ cells shown in Figure 4a,d were limited by the capacity, i.e., Li content, of the Li$_{1-x}$FePO$_4$, which (initial value) ranged from ≈1.4 to 1.6 mA cm^{-2}, depending on the current rate used. To further confirm that in the anode-free cells that Li plating/stripping on/from the Cu substrate is the limiting process, cells with a structure of Li||LiFePO$_4$ were tested using the new cycling protocol. As is clearly evident in Figure 4a, when an excess of Li is present, no capacity fading is observed and the average CE is ≈100% when the cell was charged slowly
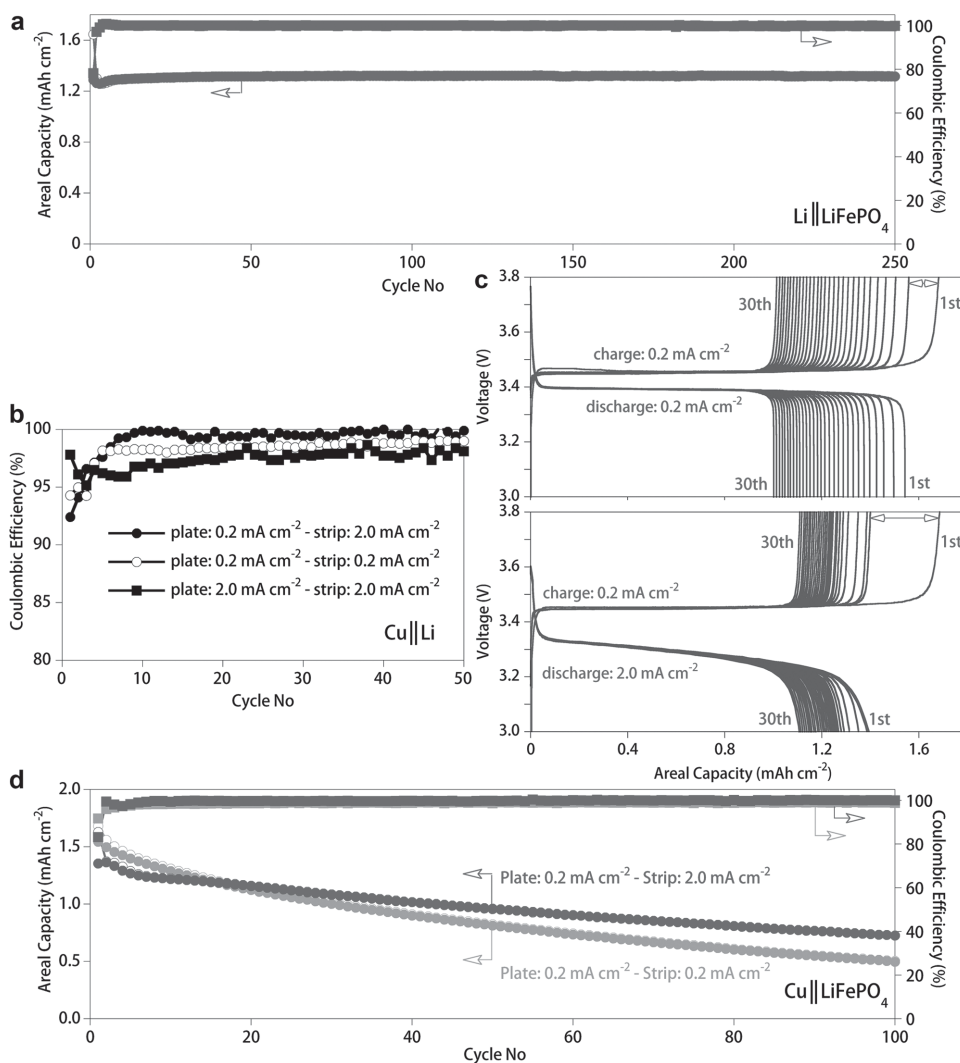
Figure 4. Cycling performance of Cu||Li and Cu||LiFePO$_4$ cells with 4 M LiFSI-DME cycled at different current densities. a) Li||LiFePO$_4$ cell cycled with low-rate (C/5) charging and high-rate (2 C) discharging. b) CE of Cu||Li cells. A capacity of 0.5 mAh cm^{-2} was used to plate the Li metal, which was subsequently stripped by cycling to 1.0 V versus Li/Li$^+$. c) Charge/discharge voltage profiles for the first 30 cycles of the anode-free cells (Cu||LiFePO$_4$) with 4 M LiFSI-DME cycled at different current densities. d) Discharge capacity and CE of anode-free Cu||LiFePO$_4$ cells charged at 0.2 mA cm^{-2} and discharged at either 0.2 or 2.0 mA cm^{-2} (open symbols: charge capacity, filled symbols: discharge capacity).

**ADVANCED
FUNCTIONAL
MATERIALS**

www.afm-journal.de

*Materials
Views*

www.MaterialsViews.com

(C/5 rate) and discharged quickly (2 C rate). Cycling the anode-free Cu||LiFePO₄ cell using the same charge/discharge protocol resulted in a notable improvement in the capacity retention. After 100 cycles, the discharge capacity was ≈54% of its original value (Figure 4d) which is a sizeable increase relative to the cells using the same current density for both charge/discharge (Figure 2b,c) which retained only ≈32% of their capacity. The average CE of the anode-free Cu||LiFePO₄ cells increased from 98.8% (for a charge/discharge at 0.2 mA cm⁻²) to 99.8% when the similar cell was cycled a low rate (0.2 mA cm⁻²) charge/high rate (2.0 mA cm⁻²) discharge protocol (Figure 4d). Although this may seem like a modest increase in the CE, Table 1 emphasizes how critical it is to achieve a nearly 100% CE to ensure the long-term cyclability of anode-free batteries, as well as other Li metal batteries.

By plating Li at low rates, large nodular deposits of Li formed which limit the surface area of the Li[19] which, in turn, limits the reactivity between the Li metal and electrolyte. Additionally, at low current density, the high concentration of anions at the Li surface which are coordinated to the Li⁺ cations (and thus more susceptible to reduction than is the case for uncoordinated anions) results in more anion decomposition (relative to solvent decomposition) and thus a higher fraction of inorganic components within the SEI.[19] Stripping the Li at high rates is also advantageous. In this case, the higher local concentration of Li⁺ produced at the surface of Li (Li → Li⁺ + e⁻), acts as a "barrier" to prevent reaction of fresh Li metal with anions and solvent molecules.[22] It is evident from both the Cu||Li and Cu||LiFePO₄ cell configurations (Figure 4b–d) that it takes ≤10 cycles for the CE (and discharge capacity) to stabilize, even with the optimized cycling protocol. A rapid stabilization of the SEI is essential for high-performance anode-free batteries and this should be the direction of future work for this type of battery.

It is worth noting that the failure rate of the anode-free cells is also affected by the cycling protocols and cell configurations. This is principally attributable to the relatively larger amount of excess Li which remains on the Cu substrate when discharging (Li stripped from the Cu substrate) at a high rate following the first charge (Li plating on the Cu) at a slow rate. This is highlighted in Figure 4c with red arrows as the excess charge capacity between the first and second cycles. When cells were cycled with little or no excess charge capacity, i.e., little to no Li remaining on the Cu, many of the anode-free cells tested failed

within a few cycles. This failure mechanism occurs when all of the Li is stripped from the Cu surface since the cell voltage regulation becomes unstable because the Cu does not serve as a stable reference to control the operating voltage of the $Li_{1-x}FePO_4$ cathode. Without a stable Li reference, the charge/discharge voltages may be out of the stability range of the $Li_{1-x}FePO_4$ resulting in the rapid degradation of the cathode. In contrast, when a larger amount of Li remained on the Cu substrate, such cell failure did not occur. Another method to obtaining reproducible anode-free cells is to use an anode current collector (Cu) which has a geometric surface area equal to or less than that of the cathode. The same failure mechanism as described above can occur if the coverage of Li is inhomogeneous on the Cu surface, which typically occurs when the anode current collector has a larger surface area than the cathode.

2.2. Electrode Evolution: X-Ray Diffraction (XRD) Analyses of the Cathode and Anode

To obtain insight into the significant differences in the performance of the anode-free cells using the two different electrolytes, cells cycled for 50 cycles were dissembled after being fully discharged and both the anode current collectors (Cu) and cathodes were analyzed by XRD to understand their structural and compositional changes. As shown in **Figure 5**a, after 50 cycles, the $Li_{1-x}FePO_4$ electrode cycled in 1 M LiPF₆-EC/DMC was completely transformed into FePO₄ with no Li remaining in the structure.[23] This indicates that the Li is completely consumed and/or trapped (as dead Li) at the anode current collector. In contrast, the $Li_{1-x}FePO_4$ cycled in 4 M LiFSI-DME consists of both LiFePO₄ and FePO₄ phases suggesting that a significant amount of the Li source is reserved and can be intercalate back into the cathode. The ratio between the LiFePO₄ and FePO₄ is estimated to be about 60:40% based upon the intensity ratio of the characteristic peaks that are assigned to LiFePO₄ (≈17°) and FePO₄ (≈18°), respectively.[23] The percentage of the un-lithiated FePO₄ is in good agreement with the capacity loss (≈40% after 50 cycles), which is principally due to the electrolyte decomposition to form the SEI layer at the anode current collector.
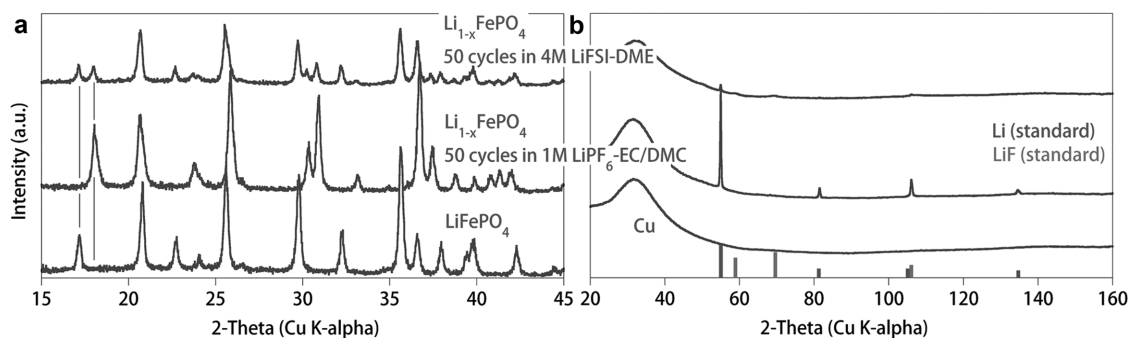
Figure 5. Post cycling analyses of the cathodes and Cu current collectors. a) XRD patterns of the $Li_{1-x}FePO_4$ cathodes after 50 cycles from cells with either 1 M LiPF₆-EC/DMC or 4 M LiFSI-DME. b) Micro-XRD analysis of the anode residues on the Cu from the same cells. Both the cathodes and Cu current collectors with residues were retrieved from the cells in the fully discharge state. The broad background peak near 32° for the micro-XRD data is due to the glass capillary tubes used for the sample containment. The bottom patterns are for the original cathode and anode current collector.

www.MaterialsViews.com

ADVANCED
FUNCTIONAL
MATERIALS
www.afm-journal.de

FULL PAPER

XRD patterns of the residues on the Cu substrates after cycling in the two electrolytes are compared in Figure 5b. The residue on the Cu collected from the cell cycled in 1 M LiPF$_6$-EC/DMC shows pronounced characteristic peaks of crystalline Li at 55°, 81°, 106°, and 135°. The Li extracted from the Li$_{1-x}$FePO$_4$ cathode is thus permanently trapped at the anode as dead Li on the Cu substrate. This accounts for the fast capacity degradation of the anode-free cell using the 1 M LiPF$_6$-EC/DMC electrolyte. In marked contrast, the XRD pattern of the residue on the Cu formed using 4 M LiFSI-DME shows only a very weak signal for crystalline Li metal. This suggests that essentially all of the unreacted Li was successfully stripped during the cell discharge and inserted back into the Li$_{1-x}$FePO$_4$, even though part of the Li extracted from the Li$_{1-x}$FePO$_4$ cathode was consumed to form SEI layer. As reported previously,[19] the SEI layer formed in the 4 M LiFSI-DME electrolyte consists predominantly of LiF. In good agreement with our previous study, the low intensity diffraction peaks here can be assigned to LiF.

2.3. Anode Morphological Evolution during Cycling

To obtain a better understanding of the evolution of the anode current collectors of the anode-free cells having different electrolytes, the morphologies of the anodes after the Li plating and of the residues on the Cu substrate after Li stripping after different cycles were further investigated. **Figure 6**a–c shows the optical photos of the Cu substrate after first cycle plating, first cycle stripping, and 50th cycle stripping, respectively, with the 1 M LiPF$_6$-EC/DMC electrolyte. Figure 6d–f shows the optical photos of the Cu substrate after first cycle plating, first cycle stripping, and 50th cycle stripping, respectively, with the 4 M LiFSI-DME electrolyte. Figure 6a1,d1 compares

the scanning electron microscopy (SEM) images of the Li film plated on the Cu substrate after the initial Li plating process Figure 6c1,2 are the top view and cross-section SEM images of the samples corresponding to Figure 6c. Figure 6f1,2 are the top view and cross-section SEM images of the samples corresponding to Figure 6f. The cells are discharged at a current density of 0.5 mA cm^{-2} for 3 h. Thus, the total amount of charge used for the Li plating was 1.5 mAh cm^{-2}, which is similar to that for the Li extracted from the LiFePO$_4$ cathode during the initial charge. As expected, the formation of needle-like dendrites of different lengths (5–10 µm) and diameters (≈200 nm to 2 µm) is observed when Li is plated in the carbonate-based electrolyte (1 M LiPF$_6$-EC/DMC) at a relatively high current density (Figure 6a1). The formation of Li dendrites is undesired in Li metal batteries because they may penetrate through the separator, causing cell short circuit and safety issues, and their high surface area results in extensive reactions with the electrolyte.[12,24] In contrast, the morphology of the Li surface plated in the 4 M LiFSI-DME electrolyte is compact and nodular, i.e., a compressed rubber-like material, which lacks the fibrous structure necessary to penetrate the porous polymer separator to generate a short-circuit (Figure 6d1).[19] The formation of these large Li particles is also favorable for suppressing the side reactions between the Li and electrolyte, due to their relatively low surface area, thus ensuring the sustainable operation of the Li metal batteries, especially those with the anode-free configuration.

Because of the limited Li source in the anode-free cells, the principal structure for the cell performance is the continuous consumption of Li in the formation/repair of the SEI layer. This SEI layer on the Li metal surface suppresses the further decomposition of the electrolyte components. However, if the SEI layer is inelastic, as is the case for the LiF-rich SEI
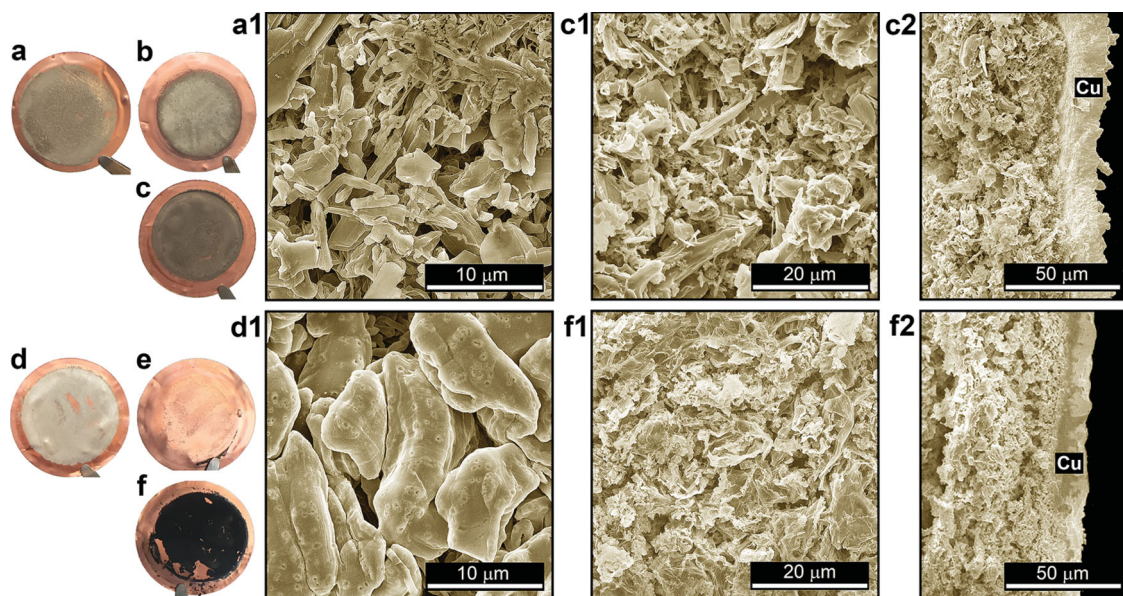
Figure 6. Optical and SEM images of the Li plating morphology and residues remaining after discharge. a–c) First cycle plating, first cycle stripping, and 50th cycle stripping, respectively, with the 1 M LiPF$_6$-EC/DMC electrolyte. d–f) First cycle plating, first cycle stripping, and 50th cycle stripping, respectively, with the 4 M LiFSI-DME electrolyte. a1,d1) The top view SEM images after first cycle plating corresponding to (a) and (d), respectively. c1,c2) The top view and cross-section SEM images corresponding to (c). f1,f2) The top view and cross-section SEM images corresponding to (f).
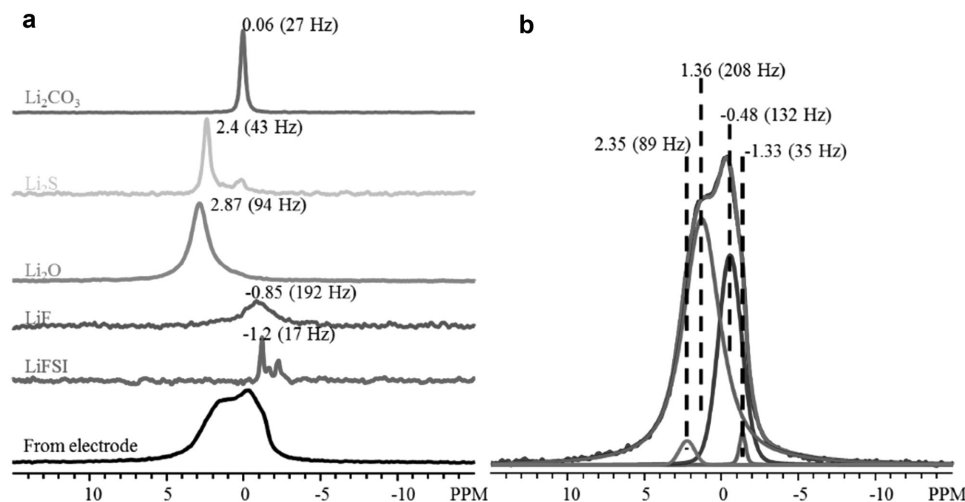
Figure 7. ^{6}Li MAS NMR spectroscopic analysis of the residues formed on the Cu substrate recovered from a cell with 4.0 M LiFSI/DME electrolyte after 50 cycles. a) Natural abundance ^{6}Li MAS NMR spectra of a series of inorganic lithium salt references and the residue and b) the corresponding fitting result of the residue (SEI byproducts) formed on the Cu substrate.

formed in 4 M LiFSI-DME, the SEI layer is disrupted in each Li plating/stripping cycle. The resulting SEI formation and reformation continuously consumes the active Li and the electrolyte, the extent of which can be quantified by measuring the CE, leading to the formation of a significant quantity of SEI residues on the Cu substrate. After 50 cycles, however, obvious differences from both optical and SEM images can be observed in the residues on the Cu substrates retrieved from the anode-free cells with the different electrolytes (Figure 6c1,f1). For the cell with 1 M LiPF$_6$-EC/DMC electrolyte, the residue after cycling looks dark gray, indicating a poor conductivity for this residual film (Figure 6c). This gray residue is actually composed of micrometer size (>10 μm) mossy/dead Li covered by a thick SEI layer (Figure 6b,c), as confirmed by the XRD characterization (Figure 5b). This is also consistent with the X-ray photoelectron analysis on the cycled Li||Cu cells that the surface layer after the initial plating of Li metal contains negligible amount of anion components, yet inorganic content (sulfur, fluoride, and nitrogen) increase during cycling due to anion degradation.[19] Since the Li metal is covered by a poorly conducting (electrically insulating) SEI layer which isolates the deposits from each other and from the Cu substrate, incomplete stripping of the SEI-wrapped Li occurs resulting in the trapping of a large amount of dead Li, leading ultimately to cell failure. In contrast, the residue on the Cu substrate after cycling in 4 M LiFSI-DME is black (Figure 6f), which is often related to a high electronic conductivity (e.g., graphite). This SEI layer, however, is also rather porous (Figure 6f). Most of the Li plated on the Cu substrate could be fully striped and reinserted into the Li$_{1-x}$FePO$_4$, except for the portion consumed by the parasitic reactions. Even after 50 cycles, only a negligible amount of Li can be identified in this residue layer (Figure 5b). Due to the low redox potential of Li (−3.04 V vs standard hydrogen electrode), the parasitic reactions between Li and the electrolyte components cannot be completely eliminated for a porous SEI which is partially disrupted during cycling, which gradually consumes the limited Li source in the anode-free cells and accumulates as reaction byproducts on the Cu substrate, resulting in the slow, but continuous capacity loss during long-term cycling.

2.4. Decomposition Byproduct of Electrolyte (4 M LiFSI/DME)

In the previous report, X-ray photoelectron spectroscopy analysis has shown that the build-up of the SEI layer formed in the 4 M LiFSI-DME electrolyte is closely related to slow anion decomposition during repeated cycling, generating a surface layer which has a significant portion of inorganic components.[18,22] Here, ^{6}Li MAS NMR was further adopted to analyze the Li-containing inorganic components of the SEI layer left as residue on the Cu substrate which was recovered from a cell with 4.0 M LiFSI/DME electrolyte after cycling (**Figure 7**). A very broad peak ranging from −10 to +10 ppm is observed for the SEI residues collected from the Cu substrate, which indicates that the SEI residues are composed of a variety of lithium salts. The fitting results of the NMR peak indicate that the inorganic components of SEI residues on the Cu substrate are composed of LiF, Li$_2$S, Li$_2$O, and a small amount of residual LiFSI salt, etc., based on their chemical shifts within the same range of the broad peak observed for SEI layer. Appearance of a significant amount of Li-containing inorganic compounds in the SEI layer enhanced the ionic conductivity and mechanical stability of the layer, in turn, the CE of Li cycling was improved.

3. Conclusion

Using a highly concentrated 4 M LiFSI-DME electrolyte, we have successfully demonstrated the efficient operation of an anode-free Li rechargeable battery (Cu||LiFePO$_4$) with a dramatically improved cycling performance relative to that achievable with a conventional carbonate-based electrolyte. A key advantage of using this highly concentrated electrolyte is the excellent

www.MaterialsViews.com

ADVANCED
FUNCTIONAL
MATERIALS
www.afm-journal.de

FULL PAPER

reversibility of the Li plating/stripping process (>99% cycling CE). The work here also demonstrates that the CE of these batteries can be even further improved by adopting a slow charge/fast discharge protocol resulting in an exceptionally high CE of more than 99.8%. The in situly formed Li (during charging) is largely stabilized due to minimized reactions between the plated Li and concentrated electrolyte. This work and the insights obtained for the SEI characteristics demonstrate a clear path forward for enabling the long sought after direct use of Li metal as a highly reversible and safe practical battery anode.

4. Experimental Section

Electrochemical Measurements: Anode-free Li rechargeable cells (Cu||LiFePO$_4$) were evaluated using CR2032 coin-type cells. These were assembled using a bare Cu foil as the anode substrate (current collector), LiFePO$_4$ coated on Al foil as the cathode, one layer of Celgard 2045 (porous polyethylene membrane) as the separator, and either 1 M LiPF$_6$-EC/DMC (1/2 v/v) or 4 M LiFSI-DME as the liquid electrolyte. Battery-grade DME was obtained from BASF Corporation. LiFSI was obtained from Nippon Shokubai and dried for 3 d under vacuum at 100 °C before use. The 4 M LiFSI-DME electrolyte was prepared by dissolving the desired amount of salt into the solvent in an MBraun LABmaster glove box with an Ar atmosphere (<1 ppm O$_2$ and <1 ppm H$_2$O). The standard LiFePO$_4$ electrode laminate was provided by A123 Systems (Waltham, MA) with a nominal areal capacity of 1.6 mAh cm^{-2}. The Cu foil substrate was washed by immersing it in 1 M HCl for 10 min, followed by rinsing with distilled water and acetone three times and then rapid drying under vacuum. All of the cell assembly/disassembly was carried out in an Ar-filled glove box. The cells were cycled between 3.0 and 3.8 V versus Li/Li$^+$ at current densities ranging from 0.2 to 2.0 mA cm^{-2} using a Lanhe battery testing station and a temperature control chamber set to 30 °C. The Cu||Li coin cells were assembled using Li foil (250 µm thick, MTI Corporation) as the counter/reference electrode, one piece of Celgard 2045 as the separator with 75 µL of electrolyte added, and Cu foil (All Foils) as the substrate for Li metal plating. The active surface area of the Cu foil disks was 2.11 cm^2. During each cycle, a capacity cut-off of 0.5 mAh cm^{-2} was used for plating and a voltage cut-off of 1.0 V (vs Li/Li$^+$) was applied for stripping. Li||LiFePO$_4$ coin cells were also assembled using Li foil (250 µm thick, MTI Corporation) as the negative electrode, one piece of polyethylene membrane (Celgard 2045) as the separator with 75 µL of electrolyte added. Disks of the LiFePO$_4$ coated on Al foil were punched with a surface area of 1.27 cm^2 to serve as the positive electrode. Cells of this configuration were cycled by charging at 0.33 mA cm^{-2} to 3.8 V and discharging at 3.3 mA cm^{-2} to 3.0 V. Electrochemical impedance spectroscopy (EIS) of the cells was measured for fully discharged cells at different stages of the cycling at a frequency range from 100 000 to 0.01 Hz with a perturbation amplitude of ±10 mV using a Solartron 1287 electrochemical interface coupled with a 1255 Frequency Response Analyzer.

Characterization: XRD of the cycled cathode (Li$_{1-x}$FePO$_4$) and anode residues on the Cu substrates recovered from the anode-free cells with the different electrolytes after 50 cycles were carried out using a D8 Advance X-ray diffractometer (Bruker AXS, Inc.) equipped with a Cu Kα source (λ = 1.5418 Å). The samples were placed in an airtight silicon crystal specimen holder (Bruker AXS, Inc.) to avoid air/moisture contamination during sample transfer for the measurements. Samples for the micro-XRD analyses were sealed under Ar in thin-walled glass capillary tubes and diffraction patterns were recorded with a Rigaku D/Max Rapid II instrument using Cr Kα radiation (λ = 2.2910 Å). The morphology studies of the Li plated on the Cu substrates and the residues on the Cu substrates after cycling (retrieved for the fully discharged cells) were performed by SEM on an FEI Quanta 650 ESEM at 5.0 kV and 0.17 nA. Natural abundance ^{6}Li NMR experiments were performed on a Varian-Inova 500 MHz NMR spectrometer equipped with a commercial 4.0 mm pencil type MAS NMR probe, operating at a magnetic field of 11.7 T with ^{6}Li Larmor frequency of 73.579 MHz. The ^{6}Li MAS spectra were acquired at sample spinning rate of 8 kHz using a single pulse sequence with a pulse angle of $\pi/4$, pulse width of 2 µs, and a recycle delay of 80 s. ^{6}Li chemical shifts were referenced to 1 M LiCl aqueous solution (0 ppm). All the NMR measurements were carried out at room temperature, i.e., 20 °C. Spectral deconvolution was carried out by fitting Lorentzian functions to the experimental spectra using the NUTs program (v.2012, Acorn NMR Inc., Las Positas, CA, USA).

[1] M. S. Whittingham, *Proc. IEEE* **2012**, *100*, 1518.
[2] J. B. Goodenough, K.-S. Park, *J. Am. Chem. Soc.* **2013**, *135*, 1167.
[3] W. Xu, J. L. Wang, F. Ding, X. Chen, E. Nasybulin, Y. Zhang, J.-G. Zhang, *Energy Environ. Sci.* **2014**, *7*, 513.
[4] D. Aurbach, E. Zinigrad, Y. Cohen, H. Teller, *Solid State Ionics* **2002**, *148*, 405.
[5] J. Jiang, W. Shi, J. Zheng, P. Zuo, J. Xiao, X. Chen, W. Xu, J.-G. Zhang, *J. Electrochem. Soc.* **2014**, *161*, A336.
[6] Y.-K. Sun, Z. Chen, H.-J. Noh, D.-J. Lee, H. G. Jung, Y. Ren, S. Wang, C. Yoon, S.-T. Myung, K. Amine, *Nat. Mater.* **2012**, *11*, 942.
[7] D. P. Wilkinson, H. Blom, K. Brandt, D. Wainwright, *J. Power Sources* **1991**, *36*, 517.
[8] F. Ding, W. Xu, G. Graff, J. Zhang, M. Sushko, X. Chen, Y. Shao, M. Engelhard, Z. Nie, J. Xiao, X. Liu, P. Sushko, J. Liu, J.-G. Zhang, *J. Am. Chem. Soc.* **2013**, *135*, 4450.
[9] G. Zheng, S. Lee, Z. Liang, H. W. Lee, K. Yan, H. Yao, H. Wang, W. Li, S. Chu, Y. Cui, *Nat. Nanotechnol.* **2014**, *9*, 618.
[10] Y. Lu, Z. Tu, L. A. Archer, *Nat. Mater.* **2014**, *13*, 961.
[11] C. M. López, J. T. Vaughey, D. W. Dees, *J. Electrochem. Soc.* **2009**, *156*, A726.
[12] R. Miao, J. Yang, X. Feng, H. Jia, J. Wang, Y. Nuli, *J. Power Sources* **2014**, *271*, 291.
[13] B. J. Neudecker, N. J. Dudney, J. B. Bates, *J. Electrochem. Soc.* **2000**, *147*, 517.
[14] J. B. Bates, N. J. Dudney, G. R. Gruzalski, R. A. Zuhr, A. Choudhury, C. F. Luck, *J. Power Sources* **1993**, *43*, 103.
[15] J. B. Bates, N. J. Dudney, D. C. Lubben, G. R. Gruzalski, B. S. Kwak, X. Yu, R. A. Zuhr, *J. Power Sources* **1995**, *54*, 58.
[16] S.-H. Lee, E. Tracy, P. Liu, *U.S. Patent 6,805,999*, **2004**.
[17] D. Wang, G. Zhong, Y. Li, Z. Gong, M. McDonald, J.-X. Mi, R. Fu, Z. Shi, Y. Yang, *Solid State Ionics* **2015**, *283*, 109.

FULL PAPER

[18] J.-J. Woo, V. Maroni, G. Liu, J. Vaughey, D. Gosztola, K. Amine, Z. Zhang, *J. Electrochem. Soc.* **2014**, *161*, A827.

[19] J. Qian, W. Henderson, W. Xu, P. Bhattacharya, M. Engelhard, O. Borodin, J.-G. Zhang, *Nat. Commun.* **2015**, *6*, 6362.

[20] D. Lv, Y. Shao, T. Lozano, W. Bennett, G. Graff, B. Polzin, J.-G. Zhang, M. Engelhard, N. Saenz, W. Henderson, P. Bhattacharya, J. Liu, J. Xiao, *Adv. Energy Mater.* **2014**, *5*, 1400993.

[21] J. Steiger, D. Kramer, R. Mönig, *Electrochim. Acta* **2014**, *136*, 529.

[22] J. Zheng, P. Yan, D. Mei, M. Engelhard, S. Cartmell, B. Polzin, C. Wang, J.-G. Zhang, W. Xu, *Adv. Energy Mater.* **2016**, *6*, 1502151.

[23] C. Delmas, M. Maccario, L. Croguennec, F. Le Cras, F. Weill, *Nat. Mater.* **2008**, *7*, 665.

[24] A. Jana, D. R. Ely, R. E. García, *J. Power Sources* **2015**, *275*, 912.